Modeling Cooling Water Discharges From the Burrard Generating Station, BC Canada

J. Jiang, D. B. Fissel and D. D. Lemon
ASL Environmental Sciences Inc.
1986 Mills Road
Sidney, BC, V8L 5Y3, Canada
asl@aslenv.com

D. Topham
Topham Scientific Consulting Services Inc.
1925 Taylor Street
Victoria, BC, V8R 3G5, Canada
dtopham@islandnet.com

***Abstract*-A three-dimensional numerical model was applied to examine the impact of the Burrard Generating Station cooling water on the circulation patterns and thermal regime in the receiving water of Port Moody Arm. A key aspect of this study involved properly incorporating the submerged cooling water buoyant jet into the 3D model. To overcome the scale and interface barriers between the near-field and far-field zones of the buoyant jet, a sub-grid scheme was applied, and the coupled system of equations of motion, heat conservation and state are solved with a single modeling procedure over the complete field. Special care was taken with the diffusion and jet entrainment by using a second order turbulence closure model for vertical diffusion and the Smagorinsky formula for horizontal diffusion as well as jet entrainment. The model was calibrated and validated in terms of buoyant jet trajectory, centerline dilution, and temperature and velocity profiles. Extensive modeling experiments without and with the Burrard Generating Station in operation were then carried out to investigate the receiving water circulations and thermal processes under the influence of the cooling water discharge. The model results reveal that under the influence of the cooling water discharge, peak ebb currents are stronger than peak flood currents in the near-surface layer, and the reverse is true in the near-bottom layer. Meanwhile, the model revealed a well-developed eddy at the southeast side of the buoyant jet in the near-surface layer. It is also found that the warmer water released from the cooling water discharge is mainly confined to the upper layer of the Arm, which is largely flushed out of the Arm through tidal mixing processes, and a corresponding inflow of colder water into the Arm occurs within the lower layer.**

I. INTRODUCTION

The Burrard Thermal Generating Station (BGS) is located on the north shore of the Port Moody Arm (hereafter, simply called the Arm), at the eastern end of the Burrard Inlet, BC, Canada (Fig. 1). The Arm has a length of 6.5 km, a mean width of 0.9 km, and the mean water depth varies from 5 to 30 m. A mixed tide occurs with a mean tidal range of 3 m. Tidal currents are mostly less than 10 – 20 cm/s. The tidal prism was computed to be 12.2×10^6 m^3, which represents approximately one-third of the total volume of the Arm [3]. BGS releases a considerable volume of heated cooling water (CW) into the Arm with a maximum allowable discharge of 1.7×10^6 m^3/d, about 14% of the tidal prism, and a maximum temperature of 27 ºC, about 4 – 10 ºC in summer and up to 20 ºC in winter above the temperature of the ambient water. This cooling water discharge into the Arm takes the form of a submerged horizontal heated buoyant jet in approximately 10 m of water depth (Fig. 1), a relatively shallow water environment.

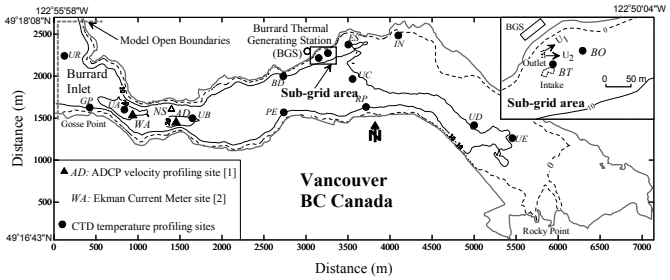

Fig. 1. Location map of the Port Moody Arm, cooling water outlet, intake, and survey sites of temperature and currents. Depths are in meters below lowest astronomical tide.

Two sets of outlet pipes are used to release the BGS cooling water discharge, namely shore side and sea side pipes (Fig. 1). Each side has two pipes of diameter 2.45 m, totaling four pipes. They are set in an identical horizontal plane with a spacing of 3 – 4 m. The elevations of the outlet pipes above the seabed are 6 m for the sea side pipes and 3 m for the shore side pipes. The outlet flows from the sea side pipes are due east. The shore side pipes are directed along the shoreline and result in an outlet flow at an angle of 20° to the east (Fig. 1). The cooling water intake is located about 30 m SSE of the outlet pipe (Fig. 1) and has opening at the height of 1.54 m – 5.88 m from the seabed with the sides facing the outlet closed. This complex combined outlet and intake structure places a particular challenge on numerical modeling.

The results of earlier two-dimensional numerical model and field investigations have shown that the cooling water has significant impact on the natural circulations and thermal regime of the receiving water body [1, 3 – 6]. Previous field investigations and studies also revealed the importance of tidal-driven exchange and mixing of the waters of Burrard Inlet in moderating the warming of the Port Moody Arm due to BGS [1, 3, 7]. However, little has been learnt so far on the features of the thermal buoyant jet and associated three-dimensional circulations and thermal regime in the receiving water. In the recent study of Burrard Generating Station cooling water recirculation by the authors of this paper [8], substantial efforts have been devoted to achieve improved insights into these behaviors using a three-dimensional numerical model: ASL-COCIRM. The model adapted a newly developed sub-grid scheme to incorporate the cooling water buoyant jet and intake properly. This paper will present the key aspects of this study, and the simulated results of the buoyant jet associated circulations and thermal processes in the receiving water.

II. MODEL FORMULATIONS

A. Governing Equations

The model solves the primitive, fully three-dimensional hydrodynamic and thermal conservation equations in a sigma-coordinate system [9, 10]. A second order turbulence closure model, as described in [11], is adapted to calculate the vertical momentum and mass diffusion coefficient. The horizontal diffusion coefficients, A_x in the x-direction and A_y in the y-direction, are evaluated using Smagorinsky formula as follows [12]

$$A_x = A_y = \frac{1}{2} C_A dx dy \sqrt{\left(\frac{\partial u}{\partial x}\right)^2 + \frac{1}{2}\left(\frac{\partial v}{\partial x} + \frac{\partial u}{\partial y}\right)^2 + \left(\frac{\partial v}{\partial y}\right)^2} \quad (2.1)$$

where C_A is an empirical coefficient, which will be determined from modeling tests in terms of buoyant jet entrainment, dx and dy respectively represent the spatial grid sizes in x- and y-directions, and u and v are the horizontal velocities in the x- and y-directions, respectively.

The boundary conditions of zero surface momentum flux (no wind stress) and bottom shear stress expressed in terms of quadratic law are employed. Measured water levels are specified at the open boundaries. At inflow, the open boundary conditions of temperature and salinity are specified from observed data, while at outflow, the conventional Sommerfeld radiation condition is used [13]. The Nikuradse's relationships were selected to specify the bottom effective roughness, z_0, with respect to turbulence strength as follows

$$\begin{cases} z_0 = k_s / 30 & \text{with} \quad u_* k_s / \upsilon > 70 \\ z_0 = 5\upsilon / u_* & \text{with} \quad u_* k_s / \upsilon < 5 \end{cases} \quad (2.2)$$

where υ is the water kinematic viscosity, k_s is the Nikuradse roughness of the bed, and u_* is the bottom friction velocity.

B. Solution Techniques

The governing hydrodynamic and thermal conservation equations are solved by the semi-implicit finite difference method in a staggered grid, which discretizes the convective and horizontal diffusive terms by an Eulerian-Lagrangian scheme [9], and the barotropic and vertical diffusive terms by an implicit method. The modeled main-domain included the whole area of the Port Moody Arm from the mouth at Burrard Inlet (Fig. 1), and was resolved using a grid-size measuring 50 m × 50 m and 10 equally spaced vertical sigma-layers. Combining the differential continuity and momentum equations, a linear, five-diagonal system of equations for the water surface elevation (ζ) is obtained as the following generalized form

$$a_{i,j}\,\zeta_{i,j}^{n+1} - a_{i+1/2,j}\,\zeta_{i+1,j}^{n+1} - a_{i-1/2,j}\,\zeta_{i-1,j}^{n+1} - a_{i,j+1/2}\,\zeta_{i,j+1}^{n+1} - a_{i,j-1/2}\,\zeta_{i,j-1}^{n+1} = b_{i,j} \quad (2.3)$$

where a and b are the coefficients dependent on hydrodynamic properties at time step n, the subscripts i and j denote the horizontal location indices and the superscript n represents the time step. This system is solved effectively by the pre-conditioned conjugate gradient method [14] along with the sub-domain in a single modeling procedure.

C. Sub-grid Scheme

In the presence of a hydraulic jet, one can classify the model domain into two characteristic zones, so called near-field and far-field. They have different spatial scales, e.g., 100 m in the near-field zone and 1000 m in the far-field zone for a typical buoyant jet. When modeling these two zones simultaneously, the scale barrier and interface coupling problem will be encountered [15]. To overcome these problems, a sub-grid scheme is applied in ASL-COCIRM, where the near-field zone of the cooling water buoyant jet and intake is nested within the far-field zone using an extremely high resolution, and these two zones are coupled together at the interface. The sub-domain has the spatial grid sizes of $dx' = dx/L$ and $dy' = dy/L$, with dx and dy denoting the spatial grid sizes of the main-domain and L representing the sub-divided step. The present sub-domain covers an area of 300×200 m^2 (Fig. 1) with L=20, which results in a horizontal resolution of 2.5 m × 2.5 m (Fig. 2). It has the identical vertical layers as the main-domain.

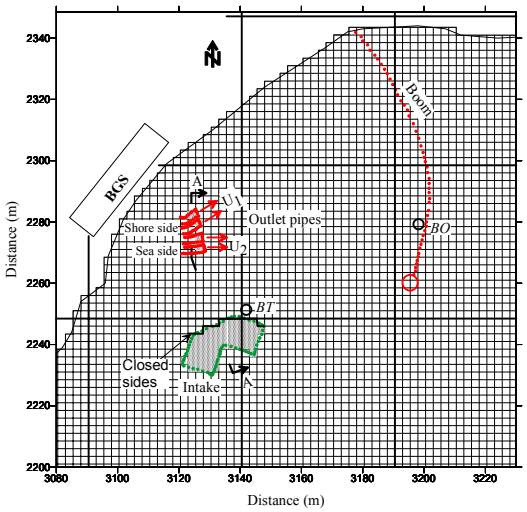

Fig. 2. Numerical plane mesh (thin lines for sub-grid and thick lines for main-grid) at the near-field, and locations of the outlet, intake, boom and temperature profiling sites BT and BO.

The extremely high resolution in the sub-domain allows the model to represent the outlet pipes and intake in a realistic manner. Certain vertical cells, two for each of the sea side pipes and three for each of the shore side pipes, are assigned as outlets, which results in cross-section areas which are approximately equal to the real ones of the outlet pipes, i.e., around 4.67 m^2 for each at mean sea level (Fig. 3). Meanwhile, the sea side outlet cells are only opened at the east sides and an eastward exit flow (U_2) results. The shore side outlet cells are opened at both the east and north sides and the resulting exit flows (U_1) will be oriented at an angle

of 20° to the east under specific discharges exiting from the east and north sides. Thus, by specifying jet discharge, exit temperature, salinity and mass concentration in these cells, the conservation of mass, thermal flux and total momentum over tidal cycles is satisfied automatically.

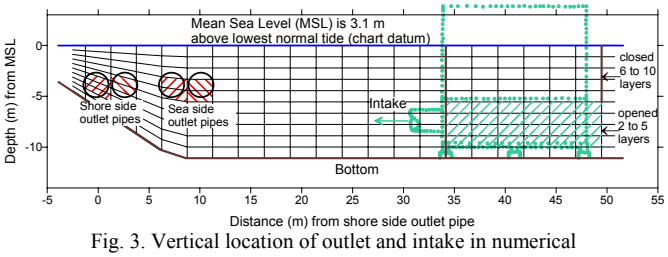

Fig. 3. Vertical location of outlet and intake in numerical mesh grid along A–A cross-section (Fig. 2).

Inside the sub-domain, the differential continuity, momentum and thermal conservation equations are the same as in the main-domain. At the interface, a coupling scheme is applied in terms of mass, momentum and thermal conservation. To ensure momentum, heat and salinity conservation at the interface, the flux forms of the momentum and thermal conservation equations are applied there. By considering mass conservation at the interface, the resulting continuity equation is related to (4+*L*) points, where four points are located in main-domain and L points at the boundary of the sub-domain. The generalized continuity equation at the interface, as shown in Fig. 4, is given in (2.4). The differential continuity equations at other interfaces will have a similar form.

$$a''_{i,j}\,\zeta^{n+1}_{i,j} - a_{i+1/2,j}\,\zeta^{n+1}_{i+1,j} - \sum_{j'=J+1}^{J+L} a'_{m+1/2,j'}\,\zeta'^{n+1}_{m,j'} - a''_{i,j+1/2}\,\zeta^{n+1}_{i,j+1} - a''_{i,j-1/2}\,\zeta^{n+1}_{i,j-1} = b''_{i,j} \tag{2.4}$$

where a' is the coefficient derived from sub-grid, ζ' is the water surface elevation at the cell centers of the sub-domain, a'' and b'' are the combined coefficients of both main- and sub-domains at the interface. Note that (2.3) and (2.4) are combined into a positive-definite linear system, it has a unique solution and is solved by pre-conditioned conjugate gradient method in all grid cells and every time step with a single modeling procedure.

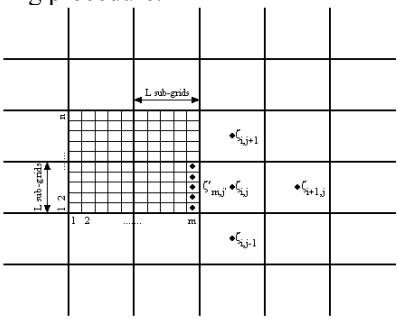

Fig. 4. Schematic diagram showing sub-grid.

The buoyant jet diffusion and entrainment are automatically included in the model using the Smagorinsky formula [12], which leads to a horizontal diffusion as a function of velocity shear, and the second order turbulence closure model. In the turbulence closure sub-model, all empirical constants were assigned the values based on the laboratory data of [11]. After adjusting the Smagorinsky coefficient through model calibrations against empirical relationship [16] and integral solutions [16, 17], the buoyant jet will be represented appropriately in the 3D model.

D. Numerical Stability

The stability of present numerical scheme is dependent on the interpolation approximation used in Eulerian-Lagrangian back tracing discretization [18] and the strength of the cooling water outlet velocity. By using a bi-linear interpolation approach, it is shown that the model will be stable with the time step

$$dt \le \mathrm{MIN}\left[\frac{U_j}{\beta(dx', dy')}, 2(A_x,\ A_y)\left(\frac{1}{(dx')^2}+\frac{1}{(dy')^2}\right)\right]^{-1} \tag{2.5}$$

where β is a constant dependent on the vertical velocity of the buoyant jet ($\beta \ge 1$), which is determined by modeling test, and U_j is the cooling water outlet velocity.

III. MODEL CALIBRATION AND VALIDATION

Before modeling the receiving water circulation and thermal regime associated with the buoyant jet of the BGS cooling water, the model was calibrated and validated using empirical relationship, integral model and field data. At first, the simulated buoyant jet under certain conditions was calibrated and validated with an empirical relationship [16] and integral model [16, 17] in terms of buoyant jet entrainment, trajectory and dilution. The modeled currents and temperatures were then compared with *in situ* observations to demonstrate the model capability of reproducing the flow and thermal fields inside the Arm.

A. Buoyant Jet

As stated above, the buoyant jet entrainment is included via the horizontal diffusion with a coefficient calculated from Smagorinsky formula [12]. The modeled entrainment was then tested against the empirical relationship introduced in [16], which assumes a buoyant jet dominated by the horizontal momentum

$$\frac{dQ}{dS} = 2\pi\alpha_j R\left|u_t\cos\psi - u_\infty\right| \tag{3.1}$$

where Q is the jet flow rate, S is the distance along the trajectory, α_j is the dimensionless entrainment coefficient with a typical value of 0.08, R is the mean jet radius, u_t is the mean of the tangential jet velocity, ψ is the angle of the trajectory with horizontal axis, and u_∞ represents the local ambient velocity. The entrainment test was carried out at a non-buoyant case and a stagnant homogenous ambient fluid, i.e., $u_\infty = 0$. The neutral jet was set at 4 m above bottom with

an outlet velocity of 2 m/s. The empirical coefficient C_A in (1.1) was adjusted until the simulated entrainment rate best-fitted (3.1). The sub-grid model ran together with the main-grid model. The resulted steady flow was used to calculate the discharge Q at different cross-sections and consequently the entrainment rate, $\Delta Q / \Delta S$. The calibrated results (Fig. 5) show that the model reasonably reproduced the entrainment rate of the buoyant jet when the empirical values of C_A=0.3 was selected. Some scatter of the simulated data is observed in Fig. 5, which is believed to be mainly caused by irregular geometry in the near-field zone (Fig. 1).

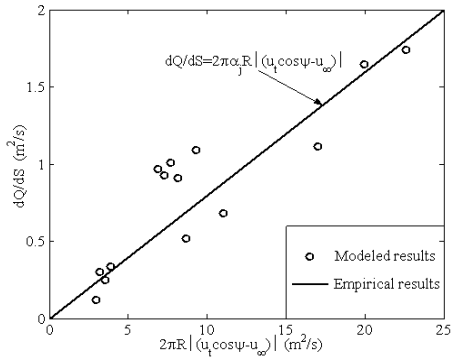

Fig. 5. Buoyant jet entrainment as a function of tangential jet velocity.

The validations of the buoyant jet trajectory, centerline velocities and temperatures were conducted under the cooling water discharge of 19.6 m^3/s, cooling water outlet velocity U_2=2.0 m/s, outlet temperature 26 °C, as well as a typical stratified environment inside the Arm during summer, and a stagnant ambient fluid. The sub-grid and main-grid models ran at the same time with the optimized parameter of C_A=0.3 until steady results were obtained. The simulated buoyancy plumes are shown in Figs. 6 and 7, which include the jet trajectory (dashed line in Fig. 6), centerline temperatures (italic numbers in Fig. 6) and centerline velocity vectors (thick vectors in Fig. 7) derived from a newly developed integral buoyant jet model as described in [16, 17]. Through comparisons with the integral model, it is seen that ASL-COCIRM predicted a very good jet trajectory, centerline velocity and temperature. The buoyant jet encounters the surface about 30 m from the outlet and then became a surface buoyant jet. The core velocity and temperature at the surfacing area are about 0.5 m/s and 19.5 °C, respectively, which are in good agreement with the integral model.

B. Vertical Structures of Velocity and Temperature

In this study, extensive model experiments were carried out to validate the hydro- and thermo-models under the identical open boundary and cooling water conditions as the observations. The simulated velocity and temperature profiles were then compared with *in situ* observations at the survey sites as shown in Fig. 1. Figs. 8 and 9 show representatives of these comparisons, i.e., the currents at the site AD and temperatures at the site BT (Fig. 1). It is seen that the model reproduced the observed vertical structures of current and temperature very well. The correlation coefficients, r, between simulated and observed results are 0.91 for currents and 0.95 for temperatures.

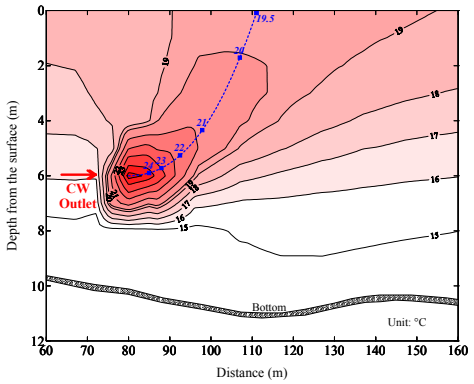

Fig. 6. Simulated thermal plume with comparisons to the integral model results of buoyant jet trajectory (dashed line) and temperatures along the jet center (italic numbers).

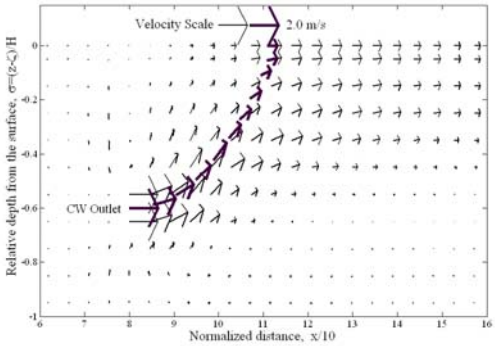

Fig. 7. Simulated buoyant jet currents (thin vectors) with comparisons to the integral model results (thick vectors) of currents along jet center.

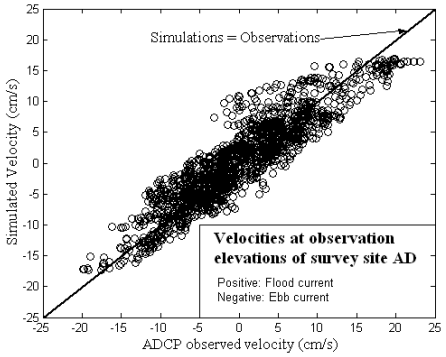

Fig. 8. Comparison between simulated and observed velocities at observation elevations of survey site AD in October, 1998.

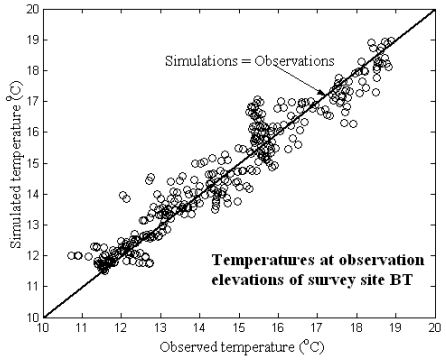

Fig. 9. Comparison between simulated and observed temperatures at observation elevations of survey site BT in October, 1998.

IV. CIRCULATIONS AND THERMAL PROCESSES UNDER THE INFLUENCE OF THE COOLING WATER DISCHARGE

From the model calibration and validation results, it is concluded that ASL-COCIRM is capable of predicting the receiving water circulations and thermal processes under the influence of the cooling water discharge. In this study, modeling of these processes was conducted at different seasons (summer, autumn and winter), different cooling water discharges (Q_{CW}), outlet velocities (U_1 and U_2), and outlet temperature (T_{CW}). In each model run, the open boundary conditions of temperature and salinity during inflow were specified using observed profile data at UR (Fig. 1), and during outflow, the conventional Sommerfeld radiation condition was applied [13]. Here, we present a representative simulation case for these model runs. Other model outputs exhibit similar thermal and circulation patterns, and thus, are not presented here. This model run dealt with summer conditions with a vertically-averaged ambient water temperature of $T_{AW} \approx 14.5$ °C and a mean ambient near-surface water temperature of about 17 °C. It has a cooling water discharge of Q_{CW} = 19.6 m^3/s and an outlet temperature of T_{CW} = 27 °C, where a cooling water discharge of 4.9 m^3/s is released through the shore side outlet pipes, which results an outlet velocity of U_1=0.5 m/s, and the remaining cooling water discharge of 14.7 m^3/s through the sea side outlet pipes, which results an outlet velocity of U_2=1.5 m/s. In order to exhibit the impact of the BGS cooling water discharge on the natural circulations and thermal regime of the receiving water, the modeled results are compared with those without the BGS in operation. The model outputs are plotted at two representative sigma-layers: the near-surface layer at 0.05H below the surface, with H denoting the total water depth, and the near-bottom layer at 0.05H above the bottom.

Fig. 10 shows the simulated peak ebb flows and temperatures without (upper panel) and with (middle and lower panels) the BGS in operation. It is observed that under the influence of the cooling water discharge, a very pronounced variation of the ebb currents is found near the surface. The submerged buoyant jet rises to the surface within 20 – 30 m of the cooling water outlet, which agrees well with the real situation [8]. After surfacing, it propagates forward in a surface buoyant jet with the core velocities of about 10 – 40 cm/s, and meanwhile gradually turns down-inlet, resulting in a stronger ebb current. Compared with those without the BGS in operation, the near-surface peak ebb currents increase by 5 – 10 cm/s with the magnitude ranging from 15 to 20 cm/s. In addition, a near-surface clockwise eddy appears at the southeast side of the buoyant jet. Near the bottom, much smaller ebb currents are found than near the surface, with the magnitude mostly less than 5 – 10 cm/s, and it is also seen that the intake withdraws cooling water from the up-inlet.

The simulated water temperatures near the surface evidently follow the flow patterns (Fig. 10). The cooling water thermal plume rises to the surface 20 – 30 m from the outlet. It is then confined to the upper layer after surfacing, and ultimately transported out of the Arm by the stronger near-surface ebb currents. In the near-field zone of the buoyant jet, the near-surface water temperature is around 19 – 20 °C, increasing by 2 – 3 °C if compared with the situation without the BGS in operation. In the far-field zone, water temperatures gradually decrease both in up-inlet and down-inlet directions. In the most areas of the receiving water, the near-surface water temperatures range from 17 – 19 °C, increasing by about 1 – 2 °C if compared with the situation without the BGS in operation. Near the bottom, the water temperatures are 14 – 15 °C, very close to the values without the BGS in operation (not shown). It implies that little heat from the cooling water is mixed down to the deeper layers.

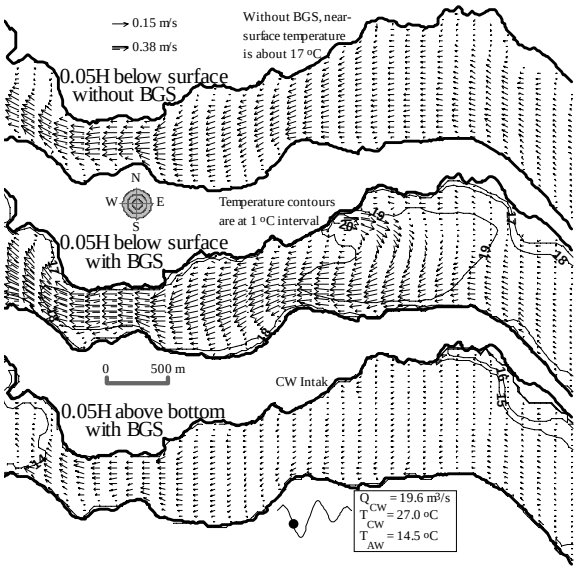

Fig. 10. Simulated peak ebb flows and temperatures at summer conditions with $T_{AW} \approx 14.5$ °C, where upper panel represents the near-surface flows without the BGS in operation, and middle and lower panels respectively represent the near-surface and near-bottom flows and temperatures with the BGS in operation under the conditions of Q_{CW} = 19.6 m^3/s, U_1 = 0.5 m/s, U_2 = 1.5 m/s, and T_{CW} = 27 °C.

During the peak flood tidal currents, the buoyant jet propagates much further up-inlet after surfacing at 20 – 30 m from the outlet (Fig. 11). At the same time, the core velocities of the surface buoyant jet slightly increase, with a range of about 10 – 45 cm/s. Down-inlet of the buoyant jet, the near-surface peak flood currents decrease by 5 – 10 cm/s if compared with those without the BGS in operation. Southeast of the buoyant jet, the near-surface flood currents appear to be entrained into the surface jet. At the near-bottom, the modeled results exhibit a stronger flood current than the ebb current, and considerable entrainment into the buoyant jet and intake. Compared with the ebb peak (Fig. 10), the near-bottom flood peak currents increase by 5 – 10 cm/s.

Such a flow pattern leads to the significant inflow of colder water into the Arm from the deeper layer, and consequently, the near-bottom temperatures inside the Arm are found to be similar to the adjoining ocean (Fig. 11), with the temperatures ranging from 14 to 15 °C. At the near-surface, the cooling water thermal plume becomes narrow

and elongated along the surface buoyant jet, and occupies a smaller area than during ebb tide (Fig. 10). Again, the near-surface water temperatures in the near-field area are about 19 – 20 °C, and 17 – 19 °C in most of far-field areas.

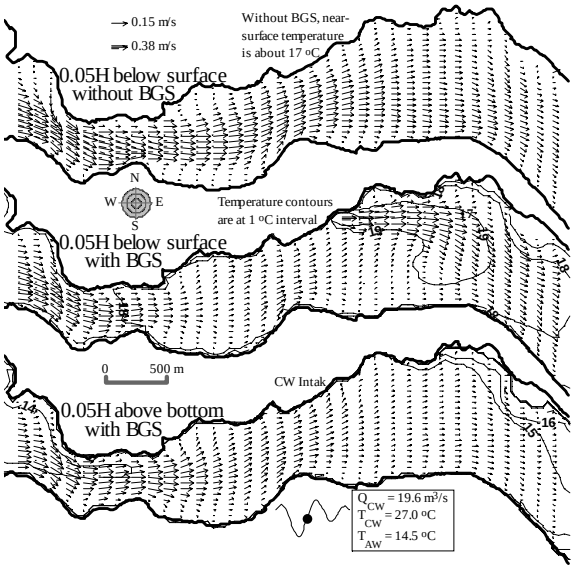

Fig. 11. Simulated peak flood flows and temperatures with the same conditions and symbol meanings as Fig. 10.

From above modeled results, it is realized that under the influence of the cooling water discharge, peak ebb currents are stronger than peak flood currents in the near-surface layer, and the reverse is true in the near-bottom layer. Therefore, the cooling water discharge will result in corresponding variation of the natural circulations of the receiving water. From the simulated residual currents (Fig. 12), it is found that without the BGS in operation, the effect of temperature and salinity induced stratification on residuals is only evident near the mouth of the Arm, where a down-inlet near-surface residual is found with the magnitude less than 2 cm/s. In other areas, the residuals seem caused by local irregular geometry, with the magnitude usually less than 1 cm/s. With the BGS in operation, a pronounced down-inlet residual occupies the most near-surface areas. At the near-bottom layer, a pronounced up-inlet residual appears, and at the same time, considerable part is entrained into the buoyant jet and intake, with the residual magnitude of 3 – 6 cm/s. In the near-field area of the buoyant jet, the near-surface residual ranges from 20 to 40 cm/s. It decreases up-inlet and gradually turns down-inlet following the geometry of the Arm and consequently leads to the down-inlet near-surface residual, with the residual currents mostly ranging from 5 – 10 cm/s. In addition, a clockwise eddy is developed to the southeast of the buoyant jet. Such a circulation pattern is consistent with a high level of heat exchange between waters of the Arm and the adjoining ocean, as modulated by the tidal forcing [1]. Consequently, the warmer water from cooling water discharge is confined to the near-surface layer, while colder water from adjoining ocean intrudes into the Arm, and thus, no noticeable effect of cooling water discharge on the near-bottom water temperatures is found from the simulations (Fig. 12).

The simulated results of the tidally-averaged thermal plume obviously follow the circulation patterns as discussed above (Fig. 12). At the near-surface layer, the tidally-averaged water temperatures are 19 – 20 °C in the near-field zone, and 17 – 19 °C in most far-field zone.

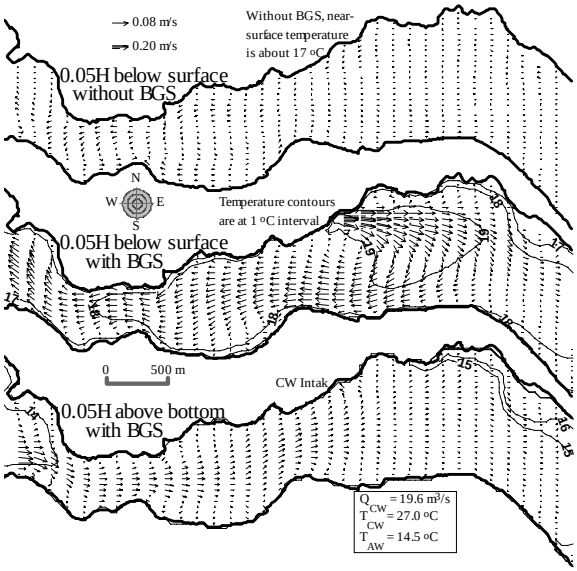

Fig. 12. Simulated residual currents and tidally-averaged temperatures under the same conditions as Fig. 10, where upper panel represents the near-surface residuals without the BGS in operation, and middle and lower panels respectively represent the near-surface and near-bottom residuals and tidally-averaged temperatures with the BGS in operation.

V. CONCLUSION AND DISCUSSION

In this study, the 3D numerical model ASL-COCIRM was extensively calibrated and validated in terms of buoyant jet trajectory, centerline dilution, and temperature and velocity profiles. The results demonstrate ASL-COCIRM's capability to predict the receiving water circulations and thermal processes under the influence of the buoyant jet in shallow receiving waters. The modeled results reveal that the submerged buoyant jet rises to the surface within 20 – 30 m of the cooling water outlet. After surfacing, the buoyant jet propagates up-inlet before it turns down-inlet. The extension distance is entirely dependent on tidal stages. As a result, the ebb currents are stronger than the flood currents in the near-surface layer, leading to a down-inlet residual flow, and the warmer water from the cooling water discharge is consequently confined to the upper layers and flushed out of the Arm effectively as modulated by the tidal forcing. It is also found that the flood currents are stronger than the ebb currents in the near-bottom layer, which leads to an up-inlet residual flow and the significant inflow of colder water into the Arm from the adjoining ocean. This result is consistent with the previous empirical conclusions derived from extensive analysis of the field observations [1].

A sub-grid model with extremely high resolution, 2.5 m by 2.5 m compared with 50 m by 50 m in the main-domain, was incorporated in present 3D model. It represented the details of outlet pipes and intake in a realistic manner. The modeled buoyant jets are in good agreement with the empirical

relationship, integral model, and field measurements in terms of jet entrainment, trajectory, dilution and surfacing location. Moreover, the model produces a detailed 3D structure of the buoyant jet. Combined with the newly developed coupling scheme, ASL-COCIRM provides a robust tool for simulating buoyant jet associated mesoscale circulations in the receiving water, waste heat removing processes and cooling water re-circulation to the intake [8].

The buoyant jet turbulence diffusion and entrainment were included through the second order turbulence closure model and the Smagorinsky formula in the model. Although needing further study, it allows the 3D model to use universally applicable approaches to simulate buoyant jet processes. Such a scheme avoids inconsistency between the sub-domain and the main-domain as well as in the vertical, and reduces assumptions as met in the case using an integral model.

ACKNOWLEDGMENTS

We thank the Burrard Generating Station, BC Hydro, for the opportunity to undertake this study, in particular Mr. Al Brotherston who supervised Burrard Generating Station Cooling Water Recirculation Study. Our thanks also extend to Dr. R. Thomson of the Institute of Ocean Sciences, and Dr. J. W. Lavelle of Pacific Marine Environmental Laboratory, NOAA, for their valuable suggestions and discussions on how to incorporate a buoyant jet into the 3D numerical model. Several other personnel at ASL assisted, in particular Alan Taylor with valuable discussions of ASL-COCIRM development and data collection. Mike Henry of the University of British Columbia made his monthly water temperature and salinity profile measurements available to this study.

REFERENCES

[1] A.E. Taylor and D.B. Fissel, *A study of the thermal regime of Port Moody Arm*, ASL Technical Report 41-399-F, ASL Environmental Sciences, Inc., Sidney, BC, Canada, p. 50, 1999.

[2] M. Waldichuk, "Water exchange in Port Moody, British Columbia, and its effect on waste disposal," *Journal of Fisheries Research Board of Canada*, vol. 22, pp. 801-822, 1965.

[3] D.B. Fissel, M. MacNeil, and A.E. Taylor, *A Study of the Thermal Regime of Port Moody Arm in Relation to the Burrard Thermal Generating Station*, ASL Technical Report 41-377-F, ASL Environmental Sciences Inc., Sidney, BC, Canada, p. 64, 1998.

[4] D.O. Hodgins and A.J. Webb, *Determination of Residual Chlorine in Burrard Inlet Originating from the Burrard Thermal Generating Plant*, Seaconsult Marine Research Ltd., Vancouver, BC, Canada, p. 55, 1991.

[5] D.O. Hodgins, *Temperature and residual chlorine measurements in Port Moody Arm*, Seaconsult Marine Research Ltd., Vancouver, BC, Canada, p. 25, 1993.

[6] Seaconsult Marine Research, *Receiving water impact assessment for the Burrard Thermal Generating Plant*. Seaconsult Marine Research Ltd., Vancouver, BC, Canada, p. 58, 1995.

[7] K.L. Birtwell, A.E. Brotherston, R.P. Fink, D.B. Fissel, J.D. Greenbank, L.I. Heithaus, J.S. Korstrom, and A.E. Taylor, *Thermal Inputs into Port Moody Arm*, *Burrard Inlet*, *BC*, *and Effects on Salmon*: *a Summary Report*, Canadian Technical Report of Fisheries and Aquatic Sciences 2340, p. 35, 2001.

[8] J. Jiang, D.B. Fissel and A. Taylor, *Burrard Generating Station Cooling Water Recirculation Study*, ASL Technical Report 41-452-f, ASL Environmental Sciences Inc., Sidney, BC, Canada, p. 45, 2001.

[9] V. Casulli and R.T. Cheng, "Semi-implicit finite-difference method for three-dimensional shallow water flow," *International Journal for Numerical Methods in Fluids*, vol. 15, pp. 629-648, 1992.

[10] A.F. Blumberg and G.L. Mellor, "A description of a three-dimensional coastal ocean circulation model," In: *Three-Dimensional Coastal Ocean Models*, N.S. Heaps ed., American Geophysical Union, Washington, DC, pp. 1-16, 1987.

[11] G.L. Mellor and T. Yamada, "Development of a turbulence closure model for geographical fluid problems," *Review of Geophysics*, vol. 20, pp. 851-875, 1982.

[12] J. Smagorinsky, "General circulation experiments with the primitive equations: I. The basic experiment," *Monthly Weather Review*, vol. 91, pp. 99-164, 1963.

[13] A. Sommerfeld, "Partial differential equations," *Lectures in Theoretical Physics*, 6, Academic Press, 1949.

[14] E. Bertolazzi, *Metodo PCG ed Applicazione ad un Modello di Acque Basse*, Thesis, University of Trento, Trento, Italy, p. 135, 1990.

[15] GESAMP (Joint Group of Experts on the Scientific Aspects of Marine Pollution), *Thermal Discharges in the Marine Environment*, Reports and Studies No. 24, Food and Agriculture Organization of the United Nations, p. 44, 1984.

[16] G.A. Bemporad, "Simulation of round buoyant jet in stratified flowing environment," *Journal of Hydraulic Engineering*, vol. 120, pp. 529-543, 1994.

[17] A.J Johnston, C.R. Phillips and R.E. Volker, "Modeling horizontal round buoyant jets in shallow water," *Journal of Hydraulic Engineering*, vol. 120, pp. 41-59, 1994.

[18] V. Casulli and E. Cattani, "Stability, Accuracy and Efficiency of a semi-implicit method for three-dimensional shallow water flow," *Computers Math. Applic.*, vol. 27, pp. 99-112, 1994.